

Entropy-Stable Discontinuous Galerkin Method for Two-Dimensional Euler Equations

M. D. Bragin^{a, *}, Yu. A. Kriksin^{a, **}, and V. F. Tishkin^{a, ***}

^a *Keldysh Institute of Applied Mathematics, Russian Academy of Sciences, Moscow, Russia*

**e-mail: michael@bragin.cc*

***e-mail: kriksin@imamod.ru*

****e-mail: v.f.tishkin@mail.ru*

Received October 22, 2020; revised October 22, 2020; accepted November 30, 2020

Abstract—A two-dimensional version of the conservative entropy-stable discontinuous Galerkin method is proposed for Euler equations in variables: density, momentum density, and pressure. For the equation describing the dynamics of the mean pressure in a finite element, an approximation is constructed that is conservative in the total energy. A special slope limiter ensures that the entropy inequality and a two-dimensional analog of the monotonicity conditions for the numerical solution are satisfied. The developed method is tested on some model gas-dynamic problems.

Keywords: Euler equations, discontinuous Galerkin method, slope limiter, entropy inequality

DOI: 10.1134/S2070048221050069

1. INTRODUCTION

Recently, the attention of researchers has been attracted by conservative entropy-stable (i.e., satisfying a discrete analog of the entropy inequality) numerical methods for solving gas dynamic problems [1–12]. One of the numerical methods that underlies the creation of entropy-stable schemes is the discontinuous Galerkin method (DGM) [13–20], which has a compact template and a potentially high approximation accuracy. Various versions of the entropy-stable modifications of the DGM, proposed to date, continue to be developed and improved. In particular, as it was established in [20] for spatially one-dimensional problems, entropy-stability should be combined with some degree of monotonicity of finite-element (FE) approximations of the DGM. This combination is achieved by constructing special limiting functions. In the case of functions of two or more spatial variables, generalizations of the concept of monotonicity are necessary, which could be successfully applied to multidimensional numerical solutions.

One of the topical areas of research is the choice of variables in which the gas dynamic equations should be numerically integrated over time in order to obtain the best result. In [21], a conservative entropy-stable spatially one-dimensional version of the DGM was proposed, in which the time integration is carried out in the variables density, momentum density, and pressure instead of the traditional set of conservative variables. In this case, in order to ensure the monotonicity requirements, limiting is carried out in relation to the DGM coefficients of pressure, and not the total energy, as was the case in the previous version [20]. As a result of this modification, it was possible to significantly improve the accuracy of the numerical solution of the Einfeldt problem [21] when calculating the specific internal energy. It is noted in [22] that methods based on the total energy conservation law sometimes lead to a poor prediction of the specific internal energy if kinetic energy is dominant. Indeed, the total energy is the sum of the internal and kinetic energies. Summation, generally speaking, leads to the loss of information about the terms. Therefore, arithmetic operations with summing can lead to a violation of the correct balance between the terms if one of them significantly exceeds another in absolute value.

This study extends the approach used in [21] for spatially one-dimensional problems to the Euler equations with two spatial variables. The variables density, momentum density, and pressure are selected due to the fact that the pair of variables, density–pressure, together with the equation of state, determines the equilibrium thermodynamic (TD) state of the gas at each point of the system, as a result of which the numerical algorithm can have a higher accuracy in describing the TD gas properties compared to the traditional use of conservative variables. Since the total energy of a perfect gas linearly depends on pressure,

the replacement of the total energy by pressure as one of the variables over which the time integration is carried out makes it easy to modify the discrete analog of the total energy conservation law so that the latter is fulfilled.

The material of the work is presented in the following sequence. Section 2 describes the formulation of the problem; Section 3 derives the DGM equations in variables of gas density, momentum density, and pressure; in Section 4, the limiting of the leading coefficients of the FE approximations is carried out, based on some generalization of the conditions of monotonicity and entropy-stability. In Section 5, the results of the numerical calculations are discussed. Section 6 contains the conclusions.

2. PROBLEM STATEMENT

We consider an initial-boundary value problem for the system of Euler equations describing two-dimensional gas dynamics in dimensionless variables:

$$\frac{\partial \mathbf{U}}{\partial t} + \frac{\partial \mathbf{F}_1(\mathbf{U})}{\partial x_1} + \frac{\partial \mathbf{F}_2(\mathbf{U})}{\partial x_2} = 0, \quad \mathbf{U}(\mathbf{x}, 0) = \mathbf{U}_0(\mathbf{x}), \tag{1}$$

$$\mathbf{x} = (x_1, x_2) \in \Pi = (a_1, b_1) \times (a_2, b_2), \quad t > 0,$$

where $\mathbf{U}(x, t) = (U^{(1)}, U^{(2)}, U^{(3)}, U^{(4)})^T$ is a column vector of conservative variables and $\mathbf{F}_j(\mathbf{U}) = (F_j^{(1)}, F_j^{(2)}, F_j^{(3)}, F_j^{(4)})^T$ is the column vector of fluxes in the direction of the Ox_j axis ($j = 1, 2$). On the boundaries of rectangle Π , certain conditions are set using ghost cells adjacent to the outside of boundary Π . The system of Eqs. (1) is closed by the equation of state for an ideal gas

$$p = (\gamma - 1)\rho\varepsilon, \quad \gamma = c_p/c_v. \tag{2}$$

The following notation is used above: p is the pressure, ρ is the density, ε is the specific internal energy, $\gamma = 1.4$ is the adiabatic exponent, and c_p and c_v are the heat capacity of an ideal gas at constant pressure and constant volume, respectively. For the momentum density and its components, as well as the total energy density, we will use the notation

$$\mathbf{I} = (I_1, I_2), \quad I_j = \rho u_j, \quad E = p/(\gamma - 1) + (I_1^2 + I_2^2)/(2\rho), \tag{3}$$

where $\mathbf{u} = (u_1, u_2)$ is the velocity vector. In the accepted notation, the column vector of conservative variables and the column vector of fluxes take the form

$$\mathbf{U} = \begin{pmatrix} \rho \\ \rho u_1 \\ \rho u_2 \\ \rho(\varepsilon + (u_1^2 + u_2^2)/2) \end{pmatrix} = \begin{pmatrix} \rho \\ I_1 \\ I_2 \\ E \end{pmatrix}, \quad \mathbf{F}_j(\mathbf{U}) = \begin{pmatrix} I_j \\ \rho^{-1} I_1 I_j + p\delta_{1,j} \\ \rho^{-1} I_2 I_j + p\delta_{2,j} \\ (E + p)\rho^{-1} I_j \end{pmatrix}, \tag{4}$$

where δ_{ij} is the Kronecker symbol.

A correct description of gas-dynamic processes presupposes the fulfillment of the entropy inequality [23] in any subdomain $\Omega \subset \Pi$ with a fairly smooth border $\partial\Omega$:

$$\iint_{\Omega} [(\rho s)(t + \Delta t) - (\rho s)(t)] d\sigma + \int_t^{t+\Delta t} d\tau \oint_{\partial\Omega} s(\mathbf{I}, d\mathbf{v}) \geq 0, \tag{5}$$

where $d\sigma$ is the area element, $d\tau$ is the element of time, $d\mathbf{v}$ is the vector element of the length, and s is the entropy density defined by the equality

$$s = \ln p - \gamma \ln \rho. \tag{6}$$

To solve problem (1), we will use an algorithm based on the DGM, a general description of which is given in [13, 16, 17]. The main features of the proposed algorithm are as follows: (a) together with the fulfillment of discrete analogs of the conservation laws, the discrete analog of the entropy inequality (5) also holds; (b) the variables of integration over time are ρ , \mathbf{I} , and p rather than the traditional set of conservative variables ρ , \mathbf{I} , and E .

3. EQUATIONS FOR DGM COEFFICIENTS IN NONCONSERVATIVE VARIABLES

In a closed computational domain $\bar{\Pi} = \Pi \cup \partial\Pi$, we define a rectangular mesh with nodes

$$\mathbf{x}_{mn} = (x_1^{(m)}, x_2^{(n)}) = (a_1 + mh_1, a_2 + nh_2), \quad m = 0, \dots, M; \quad n = 0, \dots, N, \quad (7)$$

$$\text{where } h_1 = (b_1 - a_1)/M, \quad h_2 = (b_2 - a_2)/N. \quad (8)$$

Grid (7) generates the set of computational cells $K_{mn} = (x_1^{(m-1)}, x_1^{(m)}) \times (x_2^{(n-1)}, x_2^{(n)})$, each of which has four nearest neighbors (on the sides): $K_{m-1,n}$, $K_{m,n-1}$, $K_{m+1,n}$, and $K_{m,n+1}$ with which it exchanges mass, momentum, energy, and entropy.

To describe the DGM equations in each computational cell K_{mn} , it is convenient to introduce local variables

$$z_j = 2h_j^{-1}(x_j - x_j^{(m-1)}) - 1, \quad j = 1, 2, \quad (9)$$

taking values in the interval $(-1, 1)$. When constructing the DGM, we restrict ourselves formally to the second order of approximation, presenting an approximate solution to problem (1) \mathbf{U}_h in the cell K_{mn} as a linear function of local spatial variables

$$\mathbf{U}_h(z_1, z_2, t) = \mathbf{U}_0(t) + \mathbf{U}_1(t)z_1 + \mathbf{U}_2(t)z_2. \quad (10)$$

Using the well-known technique of deriving equations for the DGM coefficients [13, 16, 17], we arrive at a system of ordinary differential equations for the desired coefficients $\mathbf{U}_0(t)$, $\mathbf{U}_1(t)$, and $\mathbf{U}_2(t)$:

$$\begin{aligned} \frac{d\mathbf{U}_0(t)}{dt} &= \mathbf{B}_0 = -h_1^{-1}[\mathbf{F}_1(1, 0, t) - \mathbf{F}_1(-1, 0, t)] - h_2^{-1}[\mathbf{F}_2(0, 1, t) - \mathbf{F}_2(0, -1, t)], \\ \frac{d\mathbf{U}_1(t)}{dt} &= \mathbf{B}_1 = -3h_1^{-1} \left[\mathbf{F}_1(1, 0, t) + \mathbf{F}_1(-1, 0, t) - \frac{1}{2} \int_{-1}^1 dz_1 \int_{-1}^1 dz_2 \mathbf{F}_1(z_1, z_2, t) \right], \\ \frac{d\mathbf{U}_2(t)}{dt} &= \mathbf{B}_2 = -3h_2^{-1} \left[\mathbf{F}_2(0, 1, t) + \mathbf{F}_2(0, -1, t) - \frac{1}{2} \int_{-1}^1 dz_1 \int_{-1}^1 dz_2 \mathbf{F}_2(z_1, z_2, t) \right]. \end{aligned} \quad (11)$$

In Eqs. (11) related to the cell K_{mn} , functions $\mathbf{F}_{1,2}$ are considered as composite functions of the corresponding local variables (9), and the exact solutions of the corresponding one-dimensional problems of discontinuity breakdown [23] are used at the cell boundaries; Godunov fluxes are applied. In this case, the integrals over each side of the rectangular cell K_{mn} are approximated by the simplest quadrature formula of rectangles with the node lying in the middle of the corresponding side.

Equations (11) describe the standard DGM. The version of the DGM proposed in this study uses Eqs. (11) to determine only the first three components of coefficients \mathbf{U}_j describing the dynamics of mass and momentum. In contrast to the traditional approach, instead of energy density $U^{(4)} = E$ as a variable of integration over time, the pressure is used, which in cell K_{mn} is also approximated by a linear function

$$p_h(z_1, z_2, t) = p_0(t) + p_1(t)z_1 + p_2(t)z_2. \quad (12)$$

Let us introduce the following notation for the kinetic energy density

$$Q(\mathbf{U}) = \frac{1}{2} \rho^{-1} \mathbf{I}^2 = \frac{1}{2} \rho^{-1} (I_1^2 + I_2^2) = \frac{1}{2} (U^{(1)})^{-1} ((U^{(2)})^2 + (U^{(3)})^2). \quad (13)$$

In what follows, it is assumed that in the right side of (13) instead of $U^{(j)}$ ($j = 1, 2, 3$) their linear approximations (10) are substituted.

Then the DGM equations for the pressure coefficients take the form

$$\begin{aligned}
\frac{dp_0(t)}{dt} = c_0 = & -(\gamma - 1) \left\{ \frac{1}{4} \int_{-1}^1 dz_1 \int_{-1}^1 dz_2 \frac{\partial Q(\mathbf{U}_h(z_1, z_2, t))}{\partial t} + h_1^{-1} [F_1^{(4)}(1, 0, t) - F_1^{(4)}(-1, 0, t)] \right. \\
& \left. + h_2^{-1} [F_2^{(4)}(0, 1, t) - F_2^{(4)}(0, -1, t)] \right\}, \\
\frac{dp_1(t)}{dt} = c_1 = & -3(\gamma - 1) \left\{ \frac{1}{4} \int_{-1}^1 z_1 dz_1 \int_{-1}^1 dz_2 \frac{\partial Q(\mathbf{U}_h(z_1, z_2, t))}{\partial t} \right. \\
& \left. + h_1^{-1} \left[F_1^{(4)}(1, 0, t) + F_1^{(4)}(-1, 0, t) - \frac{1}{2} \int_{-1}^1 dz_1 \int_{-1}^1 dz_2 F_1^{(4)}(z_1, z_2, t) \right] \right\}, \\
\frac{dp_2(t)}{dt} = c_2 = & -3(\gamma - 1) \left\{ \frac{1}{4} \int_{-1}^1 dz_1 \int_{-1}^1 z_2 dz_2 \frac{\partial Q(\mathbf{U}_h(z_1, z_2, t))}{\partial t} \right. \\
& \left. + h_2^{-1} \left[F_2^{(4)}(0, 1, t) + F_2^{(4)}(0, -1, t) - \frac{1}{2} \int_{-1}^1 dz_1 \int_{-1}^1 dz_2 F_2^{(4)}(z_1, z_2, t) \right] \right\}.
\end{aligned} \tag{14}$$

Note that the partial time derivative of the kinetic energy (13) can be found analytically taking into account Eqs. (11) for the first three components of coefficients \mathbf{U}_j .

4. NUMERICAL INTEGRATION OF EQUATIONS FOR DGM COEFFICIENTS, LIMITING AND ENTROPY-STABILITY

We consider the simplest explicit method for integrating the system of Eqs. (11) and (13) of the first order in time based on the Euler scheme. Note that the explicit Runge–Kutta methods of high orders of accuracy consist of stages similar to Euler scheme, and, in this sense, in their implementation they are reduced to it.

As noted in the previous works [13, 15–17], direct numerical integration of the system of ordinary differential equations for the DGM coefficients in the original form (11) turns out to be ineffective in a number of problems in gas dynamics. This is especially true for problems with strong shock waves. To improve the quality of the numerical solution, we resort to the regularization of the highest DGM coefficients \mathbf{U}_1 and \mathbf{U}_2 (limiting, etc.). Let us construct the method in such a way that at each time step the numerical solution satisfies discrete analogs of the laws of conservation of mass, momentum, total energy, and entropy inequality.

Note that the first equation in Eqs. (11) $d\mathbf{U}_0(t)/dt = \mathbf{B}_0$ describes some discrete analog of the laws of conservation of mass, momentum, and energy for cell K_{mn} [20] in continuous time. Its simplest difference approximation by the explicit Euler method with a time step τ

$$\mathbf{U}_0(t + \tau) = \mathbf{U}_0(t) + \tau \mathbf{B}_0(t) \tag{15}$$

also expresses the difference analog of the corresponding conservation laws, but with respect to discrete time $t = 0, \tau, 2\tau, \dots$. Therefore, we will assume that relations (15) are satisfied. The zero DGM coefficient for pressure is determined as follows:

$$\begin{aligned}
p_0(t + \tau) &= (\gamma - 1)[U_0^{(4)}(t + \tau) - Q_0(t + \tau)], \\
U_0^{(4)}(0) &= (\gamma - 1)^{-1} p_0(0) + Q_0(0),
\end{aligned} \tag{16}$$

where

$$Q_0(t) = \frac{1}{4} \int_{-1}^1 dz_1 \int_{-1}^1 dz_2 Q(\mathbf{U}_h(z_1, z_2, t)) \tag{17}$$

is a discrete analog of the average value of the gas kinetic energy in cell K_{mn} at time t .

The Euler scheme is also used to determine the leading DGM coefficients (see (13)):

$$U_k^{(j)}(t + \tau) = U_k^{(j)}(t) + \tau B_k^{(j)}(t), \quad p_k(t + \tau) = p_k(t) + \tau c_k(t), \quad (18)$$

$$j = 1, 2, 3; \quad k = 1, 2.$$

Calculation of coefficient $p_0(t)$ by formulas (16) and (17) assumes that the vector $\mathbf{U}_0(t + \tau)$ and the first three components of the coefficients $\mathbf{U}_k(t + \tau)$ ($k = 0, 1, 2$) related to density and momentum are known, but this is so in accordance with (15) and (18). After the method of numerical integration as a whole is described, let us turn to the procedure for its sequential application.

At the first stage, the limiting of the highest DGM coefficients related to the density and momentum is carried out, which is required for the stability of the numerical method. In the papers [20, 21], devoted to the solution of one-dimensional gas-dynamic problems, the importance of fulfilling the monotonicity conditions for the highest DGM coefficients is noted. For functions of many variables, the concept of monotonicity is hardly applicable, but some generalizations of it can be proposed. Let us consider one such generalization, which is close to the approach developed in [20, 21].

Assume $f = f_{mn}$ is the finite real sequence given in each cell K_{mn} , including ghost cells external to Π . Inside every cell K_{mn} lying in Π , we define the quantity

$$S_{mn}(f) = \min(|f_{m-1,n} - f_{mn}|, |f_{m,n-1} - f_{mn}|, |f_{m+1,n} - f_{mn}|, |f_{m,n+1} - f_{mn}|). \quad (19)$$

Let us denote by $\{U_0^{(j)}(t)\}$ ($j = 1, 2, 3$) the totality of all values of the zero DGM coefficients $U_0^{(j)}$ with the given index values j in all cells K_{mn} at time t . This set further plays the role of sequence f in relation (19).

Let us define the quantities

$$D_{mn}^{(1)}(t) = \min\left(\frac{\delta}{2} S_{mn}(\{U_0^{(1)}(t)\}), \sigma |U_{0,mn}^{(1)}(t)|\right), \quad (20)$$

$$D_{mn}^{(j)}(t) = \frac{\delta}{2} S_{mn}(\{U_0^{(j)}(t)\}), \quad j = 2, 3.$$

In (20) indices m and n indicate that the DGM coefficient $U_{0,mn}^{(1)}(t)$ is related to cell $K_{mn} \subset \Pi$, and δ and σ are some positive parameters.

Let us apply the limiting procedure to coefficients $U_{k,mn}^{(j)}(t + \tau)$, ($j = 1, 2, 3; k = 1, 2$), determined in accordance with (15), assuming their new values are equal to

$$\tilde{U}_{k,mn}^{(j)}(t + \tau) = \min(D_{mn}^{(j)}(t + \tau), |U_{k,mn}^{(j)}(t + \tau)|) \operatorname{sgn}(U_{k,mn}^{(j)}(t + \tau)). \quad (21)$$

At the second stage, additional limitation of the coefficients $\tilde{U}_{k,mn}^{(j)}(t + \tau)$ is made, ensuring the positive mean pressure $p_0(t + \tau)$ in cell K_{mn} . We consider the function

$$P(\lambda, t) = (\gamma - 1) \left[U_0^{(4)}(t) - \frac{1}{4} \int_{-1}^1 dz_1 \int_{-1}^1 dz_2 Q(\mathbf{V}_\lambda(z_1, z_2, t)) \right], \quad (22)$$

$$\mathbf{V}_\lambda(z_1, z_2, t) = \mathbf{U}_0(t) + \lambda [\tilde{\mathbf{U}}_1(t) z_1 + \tilde{\mathbf{U}}_2(t) z_2],$$

in which the function $Q(\mathbf{V}_\lambda)$ depends only on the first three components of the coefficients $\tilde{U}_{k,mn}^{(j)}(t + \tau)$ ($j = 1, 2, 3$) and does not depend on the fourth component $\tilde{U}_{k,mn}^{(4)}(t + \tau)$. Further, assuming that $P(0, t + \tau) > 0$, we check the condition

$$P_\sigma(\lambda) = P(\lambda, t + \tau) - \sigma P(0, t + \tau) \geq 0. \quad (23)$$

If inequality (23) is satisfied, then we put $\tilde{\lambda} = 1$, and the coefficients $\tilde{U}_{k,mn}^{(j)}(t + \tau)$ ($j = 1, 2, 3; k = 1, 2$) retain their current values. Otherwise, we find the root $\tilde{\lambda} \in [0, 1)$ of function $P_\sigma(\lambda)$ and further limit the coefficients $\tilde{U}_{k,mn}^{(j)}(t + \tau)$, replacing their current values with new values $\tilde{\lambda} \tilde{U}_{k,mn}^{(j)}(t + \tau)$. Note that the function $P_\sigma(\lambda)$ is convex upward and decreases monotonically as $\lambda \in [0, 1)$. Therefore, it is convenient to determine its root by the Newton method. In the future, after the second stage of limiting the coefficients, for convenience, we will retain their old designations $\tilde{U}_{k,mn}^{(j)}(t + \tau)$.

As a result of the second stage, the zero pressure coefficients become known

$$p_0(t + \tau) = P(\tilde{\lambda}), \tag{24}$$

and the path leads to the third stage of limiting the higher pressure coefficients $p_1(t + \tau)$ and $p_2(t + \tau)$ defined in (18). In each cell $K_{mn} \subset \Pi$ the latter are subjected to a procedure similar to (20) and (21):

$$\begin{aligned} \tilde{p}_{k,mn}(t + \tau) &= \min(D_{mn}^{(4)}(t + \tau), |p_{k,mn}(t + \tau)| \text{sgn}(p_{k,mn}(t + \tau))), \\ D_{mn}^{(4)}(t) &= \min\left(\frac{\delta}{2} S_{mn}(\{p_0(t)\}), \sigma |p_{0,mn}(t)|\right), \quad k = 1, 2. \end{aligned} \tag{25}$$

As a result of three stages of limiting, all the higher coefficients of the DGM have been determined, but the entropy stability of the method has still not been guaranteed, which ensures the fulfillment of a discrete analog of the entropy condition at each time step. The last, fourth, stage of limiting provides the entropy-stability of the proposed version of the DGM.

We consider an auxiliary function in cell $K_{mn} \subset \Pi$:

$$\begin{aligned} \Omega(\mu, t) &= \frac{1}{4} \int_{-1}^1 dz_1 \int_{-1}^1 dz_2 \rho_\mu(z_1, z_2, t) [\ln p_\mu(z_1, z_2, t) - \gamma \ln \rho_\mu(z_1, z_2, t)], \\ \rho_\mu(z_1, z_2, t) &= U_{0,mn}^{(1)}(t) + \mu(\tilde{U}_{1,mn}^{(1)}(t)z_1 + \tilde{U}_{2,mn}^{(1)}(t)z_2), \\ p_\mu(z_1, z_2, t) &= P(\mu, t) + \mu(\tilde{p}_{1,mn}(t)z_1 + \tilde{p}_{2,mn}(t)z_2), \end{aligned} \tag{26}$$

where the function $P(\mu, t)$ is determined by relation (22), and the tilde means that the higher DGM coefficients have passed through the three previous stages of limiting.

In order to calculate the expression for the discrete analog of the entropy condition (to be presented below), it is necessary to find the total numerical entropy flux (Godunov flux) across the cell boundaries K_{mn} , which is defined similarly to the right-hand sides of Eqs. (11) using the solutions of the discontinuity breakdown problem

$$\begin{aligned} \Phi_s(t) &= h_1^{-1}[F_s^{(1)}(1, 0, t) - F_s^{(1)}(-1, 0, t)] + h_2^{-1}[F_s^{(2)}(0, 1, t) - F_s^{(2)}(0, -1, t)], \\ F_s^{(j)}(z_1, z_2, t) &= (U_{0,mn}^{(j+1)}(t) + \tilde{U}_{1,mn}^{(j+1)}(t)z_1 + \tilde{U}_{2,mn}^{(j+1)}(t)z_2) [\ln(p_{0,mn}(t) + \tilde{p}_{1,mn}(t)z_1 + \tilde{p}_{2,mn}(t)z_2) \\ &\quad - \gamma \ln(U_{0,mn}^{(1)}(t) + \tilde{U}_{1,mn}^{(1)}(t)z_1 + \tilde{U}_{2,mn}^{(1)}(t)z_2)], \quad j = 1, 2. \end{aligned} \tag{27}$$

Relations (26) and (27) make it possible to obtain an explicit expression for the discrete analog of the entropy condition

$$P_s(\mu, t + \tau) = \tau^{-1}[\Omega(\mu, t + \tau) - \Omega(1, t)] + \Phi_s(t) \geq 0 \tag{28}$$

depending on the entropy-limiting parameter μ . The function on the left-hand side of equality (28) will be called *entropy production*.

Assuming that $P_s(0, t + \tau) \geq 0$, we check the fulfillment of inequality (28) for value $\mu = \tilde{\mu} = 1$. If it is fulfilled, then there is no need for entropy limiting and the current values of the higher DGM coefficients are taken as final. Otherwise, we find the root $\tilde{\mu} \in [0, 1)$ of the function $P_s(\mu, t + \tau)$ using the Newton method and further limiting the coefficients $\tilde{U}_{k,mn}^{(j)}(t + \tau)$ and $\tilde{p}_{k,mn}(t + \tau)$ ($j = 1, 2, 3; k = 1, 2$) by replacing their current values with the new values $\tilde{\mu} \tilde{U}_{k,mn}^{(j)}(t + \tau)$ and $\tilde{\mu} p_{k,mn}(t + \tau)$, and keeping their old designations for the latter.

5. CALCULATION RESULTS AND DISCUSSION

Let us test the above-constructed DGM with the entropy slope limiter on the well-known two-dimensional Riemann problems from [24]. Further, for brevity, we will call it the Entropic Slope Limiter Discontinuous Galerkin (ESLDG) scheme.

Let us describe the formulation of these problems. When carrying out numerical calculations, the following parameter values were used: $a_1 = a_2 = 0$, $b_1 = b_2 = 1$, and $M = N = 200$ in (7) and (8), the limiting parameters in (19), (22), and (24) were set equal to $\delta = 2$ and $\sigma = 10^{-5}$. The integration step was chosen in the standard way [23], based on the estimate of the maximum gas velocity in the cells. Thus, the computational domain is the square $(0, 1) \times (0, 1)$.

Table 1. Initial gas parameters and values t_{\max} in two-dimensional Riemann problems

Task		Left quarter				Right quarter				t_{\max}
		p	ρ	u_1	u_2	p	ρ	u_1	u_2	
4	Upper	0.35	0.5065	0.8939	0	1.1	1.1	0	0	0.25
	Bottom	1.1	1.1	0.8939	0.8939	0.35	0.5065	0	0.8939	
6	Upper	1	2	0.75	0.5	1	1	0.75	-0.5	0.3
	Bottom	1	1	-0.75	0.5	1	3	-0.75	-0.5	
17	Upper	1	2	0	-0.3	1	1	0	-0.4	0.3
	Bottom	0.4	1.0625	0	0.2145	0.4	0.5197	0	-1.1259	

At the initial moment of time ($t = 0$), the computational domain is divided into four equal parts, each of them has its own constant distribution of gas parameters specified. The symmetry conditions are set at the boundaries of the computational domain. It is required to calculate the gas flow until $t = t_{\max}$ inclusive.

Of all the two-dimensional Riemann problems available in [24], we will consider cases 4, 6, and 17. The initial gas parameters and values t_{\max} for them are given in Table 1.

In addition, we will make a comparison with the locally one-dimensional bcompact scheme SDIRK3B4 [25, 26] of the fourth order of approximation in space and the second order of approximation in time. Calculations by the bcompact scheme will be carried out using the conservative limiting method [26] (the parameter of this method $C_1 = 10$) on the same grid with the Courant number 0.8. In the calculations using the ESLDG scheme, a smaller time step (Courant number 0.2) was chosen, since in the current implementation this scheme has the first order of approximation.

Case 4. The lines of initial discontinuities in this problem are shock fronts. Over time, from the point of their initial convergence, a new region of continuous flow is formed, which has the shape of a lens and is bounded by two shock waves. The choice of this particular test problem is due to the fact that its solution has no other strong discontinuities, except for the aforementioned six shock waves; this makes it possible to examine the schemes separately only on jumps of this type.

Figure 1 shows for $t = t_{\max}$ the entropy production rate P_s and solution (parameters p , ρ , u_1 , u_2) for the ESLDG scheme, as well as the solution calculated according to the SDIRK3B4 scheme. It can be seen that the entropy slope limiter of the ESLDG scheme ensures the inequality $P_s \geq 0$ in all cells of the grid; therefore, it meets its purpose. Note that the ESLDG scheme has a large numerical dissipation in comparison with the bcompact SDIRK3B4 scheme: this can be understood from the thickness of shock waves and from the shape of the density isolines in the lens region. The plot of P_s confirms that the maximum entropy production, or dissipation, is concentrated at the shock fronts.

Case 6. The lines of initial discontinuities in this problem are surfaces of moving tangential shocks. Their movement leads to the appearance of a zone of moderate gas rarefaction in the form of a parallelo-

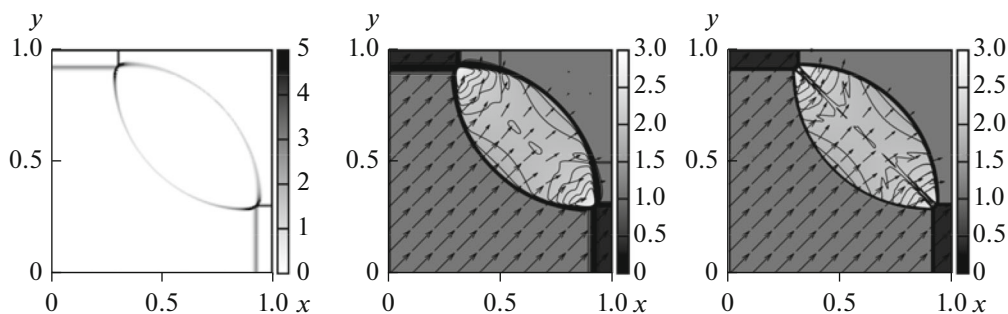


Fig. 1. Results in Case 4, time $t = 0.25$. Left: ESLDG entropy production. In the center: pressure (color fill), density (isolines from 0.52 to 1.92 with a step of 0.05), velocity (vectors in a scale of 0.1), obtained using the ESLDG scheme. Right: the same, obtained using the SDIRK3B4 bcompact scheme. Calculations for both schemes are performed on a grid of 200×200 cells.

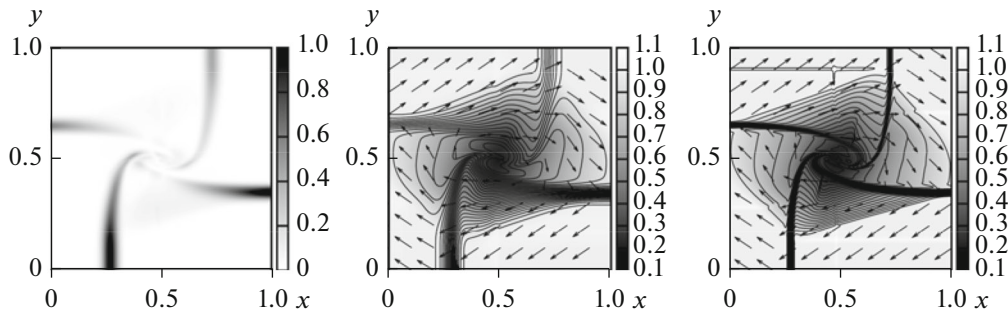


Fig. 2. Results in Case 6, time $t = 0.3$. Left: ESLDG entropy production. In the center: pressure (color fill), density (iso-lines from 0.25 to 3.05 with a step of 0.1), velocity (vectors in a scale of 0.1), obtained using the ESLDG scheme. Right: the same obtained using the SDIRK3B4 bicomcompact scheme. Calculations for both schemes are performed on a grid of 200×200 cells.

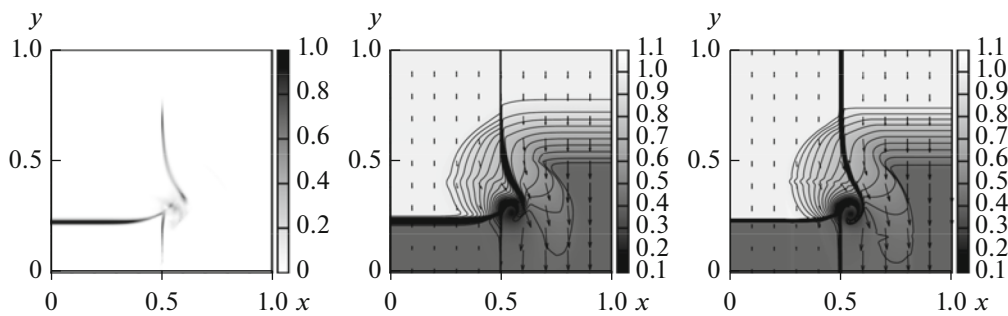


Fig. 3. Results in Case 17, time $t = 0.3$. Left: ESLDG entropy production. In the center: pressure (color fill), density (iso-lines from 0.54 to 1.99 with a step of 0.05), velocity (vectors in a scale of 0.08) obtained using the ESLDG scheme. Right: the same obtained using the SDIRK3B4 bicomcompact scheme. Calculations for both schemes are performed on a grid of 200×200 cells.

gram. The potential for the appearance of nonphysical rarefaction shocks in it and the difficulty of accurately resolving tangential discontinuities served as the motivation for choosing this particular test.

The flows obtained by both schemes and the field P_s at the moment $t = t_{\max}$ are visualized in Fig. 2. The ESLDG scheme again has nonnegative entropy production. However, its numerical dissipation quite noticeably smears the fronts of the tangential discontinuities when compared with the SDIRK3B4 scheme (more than 20 cells versus 5–6 cells). Similarly to Case 4, the largest entropy production falls on strong discontinuities in the flow parameters.

Case 17. In this test, both vertical initial discontinuities are tangential jumps, and the left horizontal discontinuity is a shock wave. After the initial moment of time, the right horizontal discontinuity turns into a rarefaction wave. In the vicinity of the point of convergence of the shock wave and both tangential jumps, there is a moderate rarefaction of the gas. An interesting feature of the flow is that, far from this circular rarefaction zone, both tangential discontinuities remain motionless while near them they experience a slow displacement. This feature, as well as the presence of two other signature gas-dynamic structures, a shock wave and a rarefaction wave, explain the choice of this particular test problem.

Figure 3 shows the plot of P_s and flow pictures at $t = t_{\max}$. It is important that the entropy regularization algorithm in the ESLDG scheme ensures the fulfillment of a discrete analog of the entropy inequality. The fixed sections of tangential discontinuities are resolved by the ESLDG scheme on one cell (in the transverse direction), which is explained by the well-known property of the Godunov flux. The SDIRK3B4 bicomcompact scheme smears out these regions, since it uses the global Lax–Friedrichs flux splitting. However, it better resolves shock waves and moving tangential discontinuities.

6. CONCLUSIONS

(1) A conservative entropy-stable version of the discontinuous Galerkin method (ESLDG) is formulated for the Euler equations with two spatial variables, in which the time integration takes place in non-conservative variables: density, momentum density, and pressure.

(2) The proposed version of the DGM can be easily generalized to equations with three spatial variables.

(3) The developed numerical algorithm and the corresponding computer program for performing numerical calculations were verified on test problems in [24]. The tests carried out have shown satisfactory results. The advantage of the proposed ESLDG method is nonnegative entropy production.

(4) Although, as it turned out, a high-order accurate bcompact scheme, as a rule, has a better spatial resolution than the ESLDG. A further improvement in the quality of the numerical solution with the ESLDG scheme is possible by increasing its approximation order and by improving the procedure for limiting the higher DGM coefficients, which is supposed to be carried out in future studies.

ACKNOWLEDGMENTS

The authors thank the supercomputer center of the Research Computing Center of the Lomonosov Moscow State University and the Center for Information Technology of the University of Groningen (Netherlands) for the opportunity to perform the calculations.

FUNDING

This study was supported by the Russian Science Foundation, project no. 17-71-30014.

REFERENCES

1. E. Tadmor, “Entropy stable schemes,” *Handb. Numer. Anal.* **17**, 467–493 (2016).
2. P. D. Lax, *Hyperbolic Systems of Conservation Laws and the Mathematical Theory of Shock Waves* (SIAM, Philadelphia, 1973).
3. S. Osher, “Riemann solvers, the entropy condition, and difference approximations,” *SIAM J. Numer. Anal.* **21**, 217–235 (1984).
4. F. Bouchut, C. Bourdarias, and B. Perthame, “A MUSCL method satisfying all the numerical entropy inequalities,” *Math. Comput.* **65**, 1439–1461 (1996).
5. E. Tadmor, “Entropy stability theory for difference approximations of nonlinear conservation laws and related time-dependent problems,” *Acta Numerica* **12**, 451–512 (2003).
6. F. Ismail and P. L. Roe, “Affordable, entropy-consistent Euler flux functions II: Entropy production at shocks,” *J. Comput. Phys.* **228**, 5410–5436 (2009).
7. P. Chandrashekar, “Kinetic energy preserving and entropy stable finite volume schemes for compressible Euler and Navier–Stokes equations,” *Comm. Comput. Phys.* **14**, 1252–1286 (2013).
8. U. S. Fjordholm, S. Mishra, and E. Tadmor, “Arbitrarily high-order accurate entropy stable essentially nonoscillatory schemes for systems of conservation laws,” *SIAM J. Numer. Anal.* **50**, 544–573 (2012).
9. X. Cheng and Y. Nie, “A third-order entropy stable scheme for hyperbolic conservation laws,” *J. Hyperbolic Differ. Equations* **13**, 129–145 (2016).
10. V. V. Ostapenko, “Symmetric compact schemes with artificial viscosities of increased order of divergence,” *Comput. Math. Math. Phys.* **42**, 980–999 (2002).
11. A. A. Zlotnik, “Entropy-conservative spatial discretization of the multidimensional quasi-gasdynamic system of equations,” *Comput. Math. Math. Phys.* **57**, p.706–725 (2017).
12. G. J. Gassner, A. R. Winters, and D. A. Kopriva, “A well balanced and entropy conservative discontinuous Galerkin spectral element method for the shallow water equations,” *Appl. Math. Comput.* **272**, 291–308 (2016).
13. B. Cockburn, “An introduction to the Discontinuous Galerkin method for convection-dominated problems,” in *Advanced Numerical Approximation of Nonlinear Hyperbolic Equations*, Ed. by A. Quarteroni, Lecture Notes in Mathematics (Springer, Berlin, 1997), Vol. 1697, pp. 150–268.
14. M. E. Ladonkina, O. A. Neklyudova, and V. F. Tishkin, “Application of averaging to smooth the solution in DG method,” KIAM Preprint No. 89 (Keldysh Inst. Appl. Math., Moscow, 2017) [in Russian]. <http://library.keldysh.ru/preprint.asp?id=2017-89>.
15. M. E. Ladonkina, O. A. Neklyudova, and V. F. Tishkin, “Impact of different limiting functions on the order of solution obtained by RKDG,” *Math. Models Comput. Simul.* **5**, 346–349 (2013).

16. M. E. Ladonkina and V. F. Tishkin, “Godunov method: a generalization using piecewise polynomial approximations,” *Differ. Equations* **51**, 895–903 (2015).
17. M. E. Ladonkina and V. F. Tishkin, “On Godunov-type methods of high order of accuracy,” *Dokl. Math.* **91**, 189–192 (2015).
18. V. F. Tishkin, V. T. Zhukov, and E. E. Myshetskaya, “Justification of Godunov’s scheme in the multidimensional case,” *Math. Models Comput. Simul.* **8**, 548–556 (2016).
19. Y. A. Kriksin and V. F. Tishkin, “Entropic regularization of Discontinuous Galerkin method in one-dimensional problems of gas dynamics,” KIAM Preprint No. 100 (Keldysh Inst. Appl. Math., Moscow, 2018) [in Russian]. <http://library.keldysh.ru/preprint.asp?id=2018-100>.
20. M. D. Bragin, Y. A. Kriksin, and V. F. Tishkin, “Discontinuous Galerkin method with an entropic slope limiter for Euler equations,” *Math. Models Comput. Simul.* **12**, 824–833 (2020).
21. Y. A. Kriksin and V. F. Tishkin, “Numerical solution of the Einfeldt problem based on the discontinuous Galerkin method,” KIAM Preprint No. 90 (Keldysh Inst. Appl. Math., Moscow, 2019) [in Russian]. <http://library.keldysh.ru/preprint.asp?id=2019-90>.
22. A. C. Robinson, T. A. Brunner, S. Carroll et al., “ALEGRA: An arbitrary Lagrangian-Eulerian multimaterial, multiphysics code,” in *46th AIAA Aerospace Sciences Meeting and Exhibit* (Reno, NV, 7–10 January 2008), p. 2008-1235 (2008). <https://doi.org/10.2514/6.2008-1235>.
23. S. K. Godunov, A. V. Zabrodin, M. Ya. Ivanov, A. N. Kraiko, and G. P. Prokopov, *Numerical Solution of Multidimensional Problems of Gas Dynamics* (Nauka, Moscow, 1976) [in Russian].
24. R. Liska and B. Wendroff, “Comparison of several difference schemes on 1D and 2D test problems for the Euler equations,” *SIAM J. Sci. Comput.* **25**, 995–1017 (2003).
25. M. N. Mikhailovskaya and B. V. Rogov, “Monotone compact running schemes for systems of hyperbolic equations,” *Comput. Math. Math. Phys.* **52**, 578–600 (2012).
26. M. D. Bragin and B. V. Rogov, “Conservative limiting method for high-order bcompact schemes as applied to systems of hyperbolic equations,” *Appl. Numer. Math.* **151**, 229–245 (2020).